engineering proceedings

MDPI

Proceeding Paper

Simple Experimental Evaluation of a Quantum Computer via Tomography and GHz States †

Darin Peev * and Yordan Sivkov

Department of Electronics, Nikola Vaptsarov Naval Academy, 9002 Varna, Bulgaria; jsivkov@naval-acad.bg

* Correspondence: d.peev@naval-acad.bg; Tel.: +359-882-412-447

† Presented at the 6th International Conference on Communications, Information, Electronic and Energy Systems, 26–28 November 2025, Ruse, Bulgaria.

Abstract

This paper presents a simple experimental method for evaluating a superconducting quantum processor through two-qubit quantum state tomography and generalized GHZ-state benchmarking. The goal is to provide an accessible procedure for assessing hardware fidelity and entanglement capability. The method was demonstrated using IBM's 127-qubit ibm_brisbane device, where each Bell state was prepared and reconstructed from 10,000 shots, and the resulting fidelities were compared to Qiskit Aer simulations. The method further examines multi-qubit GHZ states to gauge scalability. The main advantages are its simplicity, reproducibility on free IBM Quantum hardware, and its suitability for entry-level experimentation and performance evaluation.

Keywords: quantum computing; quantum state tomography; Qiskit; IBM Quantum; density matrix; quantum state fidelity; bell states

1. Introduction

Although quantum computers are still in their infancy today, they possess a number of unique properties that distinguish them from their classical counterparts. In 2019, Google announced that it had executed a quantum algorithm which would take a classical computer an estimated 10,000 years to complete [1]. The advantage of the quantum computer does not lie in component miniaturization necessarily or access speed. In fact, in terms of these two factors, the current hardware implementation of a quantum computer is significantly less efficient than that of traditional classical computers.

What makes the superiority of quantum computing possible is its access to quantum properties of information, which are radically different from those in the macroscopic world. Like a classical computer, a quantum computer can process information in binary form. However, while a classical bit exists as either a 0 or a 1 at any given moment, depending on the voltage of the signal encoding it, a qubit can occupy a superposed state combining 0 and 1, with different probabilities and a specific phase associated with each component. The phase arises from the fact that quantum systems also exhibit wave-like behavior. There are various methods for encoding a quantum state, such as the polarization of photons or the quantum spin of electrons [2].

Quantum computing is rapidly evolving, driven by foundational breakthroughs like Shor's factoring algorithm to recent advances in certified randomness and quantum sampling. Central to this progress is the ability to accurately prepare, manipulate, and measure quantum states—a capability that underpins tasks such as quantum cryptography,

Check for updates

Academic Editors: Teodor Iliev, Ivaylo Stoyanov and Grigor Mihaylov

Published: 14 January 2026

Copyright: © 2026 by the authors. Licensee MDPI, Basel, Switzerland. This article is an open access article distributed under the terms and conditions of the Creative Commons Attribution (CC BY) license.

and quantum machine learning. The Bell states are among the most fundamental quantum configurations. They exhibit maximal entanglement and are critical for demonstrating quantum nonlocality, teleportation, and superdense coding [3,4].

By enabling the generation and distribution of entanglement across many interconnected nodes, quantum communication networks—realized through optical interactions involving single photons—offer a means to detect eavesdropping through Bell's theorem [5]. The possibility for a free-space quantum communication based on entanglement has been shown, even in daylight rain conditions in urban areas.

Future quantum internet could utilize a variety of photonic technologies, such as quantum repeaters and satellite-based entanglement. Satellite-based quantum key distribution on entanglement has already been successfully demonstrated and utilized.

Various architectures can link high-precision quantum sensors with a quantum computer for data processing. In an example scenario, each quantum sensor is paired with a small local quantum module that performs limited quantum pre-processing and converts the result into classical data, which is then sent to a remote quantum computer or cloud for further analysis.

This paper explores quantum state tomography for characterizing entanglement on an IBM quantum computer. State tomography, which involves reconstructing the complete state of a quantum system from measurement data, is essential for assessing the accuracy and guiding the development of quantum technologies [6–8]. With advances in quantum processor architectures, tomography is an important tool for analyzing coherence properties, evaluating gate performance, and characterizing entanglement within the system [6].

The IBM Quantum platform used in this work offers free cloud-based access to actual quantum processors, enabling users to run experiments on physical quantum hardware [9]. It is seamlessly integrated with Qiskit, an open-source quantum programming framework developed by IBM for building, simulating, and executing quantum programs in Python. In this work, Python version 3.12.4 and Qiskit versions 1.2.4 and 1.3.1 were used [10–12]. Together, IBM Quantum and Qiskit form a user-friendly environment for developing, testing, and deploying quantum algorithms.

In this work, we used ibm_brisbane, belonging to the IBM's Quantum Eagle r3 series of processors.

The quantum state fidelities reported in this work were obtained directly from the quantum hardware, and, for simulations, from the Aer simulator.

2. Materials and Methods

2.1. Basic Theory

In general, the state vector for a two-qubit system according to Dirak notation [13] is

$$|\psi\rangle = \alpha_{00}|00\rangle + \alpha_{01}|01\rangle + \alpha_{10}|10\rangle + \alpha_{11}|11\rangle, \quad (1)$$

with the normalization condition concerning the probability amplitudes

$$|\alpha_{00}|^2 + |\alpha_{01}|^2 + |\alpha_{10}|^2 + |\alpha_{11}|^2 = 1. \quad (2)$$

The four maximally entangled pure states are

$$|\Phi^+\rangle = (1/\sqrt{2}) \begin{pmatrix} 1 \\ 0 \\ 0 \\ 1 \end{pmatrix}, \quad (3)$$

https://doi.org/10.3390/engproc2026122005

$$|\Phi^-\rangle = (1/\sqrt{2}) \begin{pmatrix} 1 \\ 0 \\ 0 \\ -1 \end{pmatrix}, \tag{4}$$

$$|\Psi^+\rangle = (1/\sqrt{2}) \begin{pmatrix} 0 \\ 1 \\ 1 \\ 0 \end{pmatrix}, \tag{5}$$

$$|\Psi^-\rangle = (1/\sqrt{2}) \begin{pmatrix} 0 \\ 1 \\ -1 \\ 0 \end{pmatrix}. \tag{6}$$

They are known as Bell states, named after the renowned physicist John Bell. A generalized state involving n entangled qubits is [14]

$$|GHZ_n\rangle = \left(1/\sqrt{2}\right) \left(|0\rangle^{\otimes n} + |1\rangle^{\otimes n}\right) \tag{7}$$

Entangled qubits are successfully used for establishing secure communications and they are widely used in quantum cryptography [14].

2.2. Quantum State Tomography, Density Matrix and State Fidelity

The application of state vectors in describing quantum states does not extend beyond states termed pure states. In cases when a state vector $|\psi\rangle$ does not occur with probability 1, i.e., the state is not pure, a generalized description is provided through the so-called density matrix. If the actual state is unknown, but several pure states $|\psi_i\rangle$ are candidates instead, each with its corresponding probability of occurring p_i, the system's state is described by the following density matrix ρ [6–8]:

$$\rho = \sum_{i=1}^{N} p_i |\psi_i\rangle\langle\psi_i| \tag{8}$$

with N being the number of possible pure states in the list. Several types of measurements are required to form a complete picture of a quantum state. Each type of measurement then serves as a "different observation angle" to reconstruct the "object in its entirety". That process is called quantum state tomography, from the Greek word tomos—section. Exactly in this capacity of encompassing the complete description that is accessible, quantum tomography is indispensable. It uses a sufficient basis of measurement operators and multiple shots to reconstruct the quantum state.

By introducing a type of distance measure, the closeness of two quantum states can be evaluated for the purpose of quantifying the quality of a quantum algorithm implementation. It relates to the overlap between a pure desired state and an arbitrary state. The general formulation [6] is as follows:

$$F(\rho, \sigma) = \left(Tr\left\{\sqrt{\sqrt{\rho}\sigma\sqrt{\rho}}\right\}\right)^2 \tag{9}$$

where for either matrix being a pure state it works out as $Tr\{\rho\sigma\}$ [6].

A significant contributor to the loss of performance in a quantum system is decoherence due to undesired influences, incl. environmental [15].

https://doi.org/10.3390/engproc2026122005

3. Results of Two-Qubit Quantum State Tomography on IBM Quantum Computer for the Four Bell States

The preparation of the four Bell states follows distinct gate sequences, while the measurement and analysis procedure remains identical. To generate $|\Phi^+\rangle$, qubit q_0 is subjected to a Hadamard gate, after which a controlled-NOT gate with q_0 being the control and q_1 the target is applied. The state $|\Phi^-\rangle$ is obtained by applying an X gate and a Hadamard gate to q_0, followed by the same CNOT operation. For $|\Psi^+\rangle$, a Hadamard gate is applied to q_0 and an X gate to q_1. The last circuit stage is an identical CNOT gate. Finally, $|\Psi^-\rangle$ is prepared by applying a Hadamard on q_0, an X gate on q_1, and Z gates on both qubits, before completing the circuit with analagous CNOT.

In all cases, the density matrix $\rho = |\psi\rangle\langle\psi|$ of the target state is reconstructed through quantum state tomography on the ibm_brisbane device using 10,000 shots. The experimentally measured fidelities, listed in Table 1, are compared with ideal states simulated using Qiskit Aer (see the description of Table 1).

Table 1. Measured quantum fidelities (Fidelity_M) executed on the ibm_brisbane quantum computer and fidelities from the Qiskit Aer simulator (Fidelity_S) for the four Bell states.

Index	Fidelity_M	Fidelity_S
$\|\Phi^+\rangle$	0.8735	0.9972
$\|\Phi^-\rangle$	0.8513	0.9983
$\|\Psi^+\rangle$	0.8688	0.9954
$\|\Psi^-\rangle$	0.8625	0.9918

The graphical representation of these results is presented in Figure 1. The differences between the experimentally obtained density matrix and the one acquired by simulation are shown in Figure 2 element by element. The discrepancies reflect the effect of noise and device imperfections, providing a more realistic estimate of hardware performance than gate-level fidelity values alone. The maximum absolute differences in the density matrix elements between real hardware measurements and Aer simulation were evaluated separately for the real and imaginary parts. For the first Bell state $|\Phi^+\rangle$, the real and imaginary parts are 0.0824 and 0.0174, respectively; for the second Bell state $|\Phi^-\rangle$, 0.1013 and 0.0128; for the third Bell state $|\Psi^+\rangle$, 0.0842 and 0.0223; and for the fourth Bell state $|\Psi^-\rangle$, 0.0870 and 0.0265. The values for the real part align with the measured fidelities—the larger the differences, the lower the fidelity. The imaginary parts do not exhibit a clear trend; in this case they mainly reflect noise. That is expected since the ideal density matrices of the Bell states have zero imaginary entries.

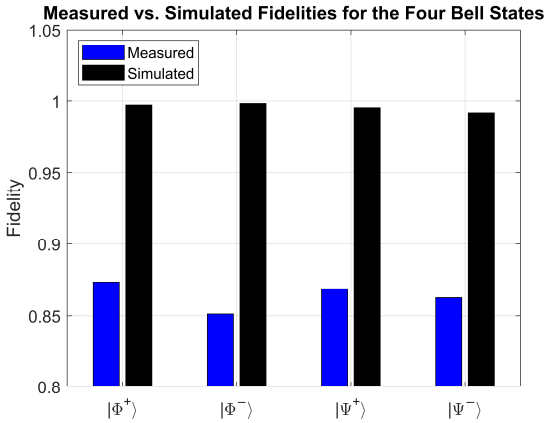

Figure 1. Fidelities of the four Bell states obtained experimentally (blue) for the ibm_brisbane quantum computer and from Qiskit Aer simulation (black).

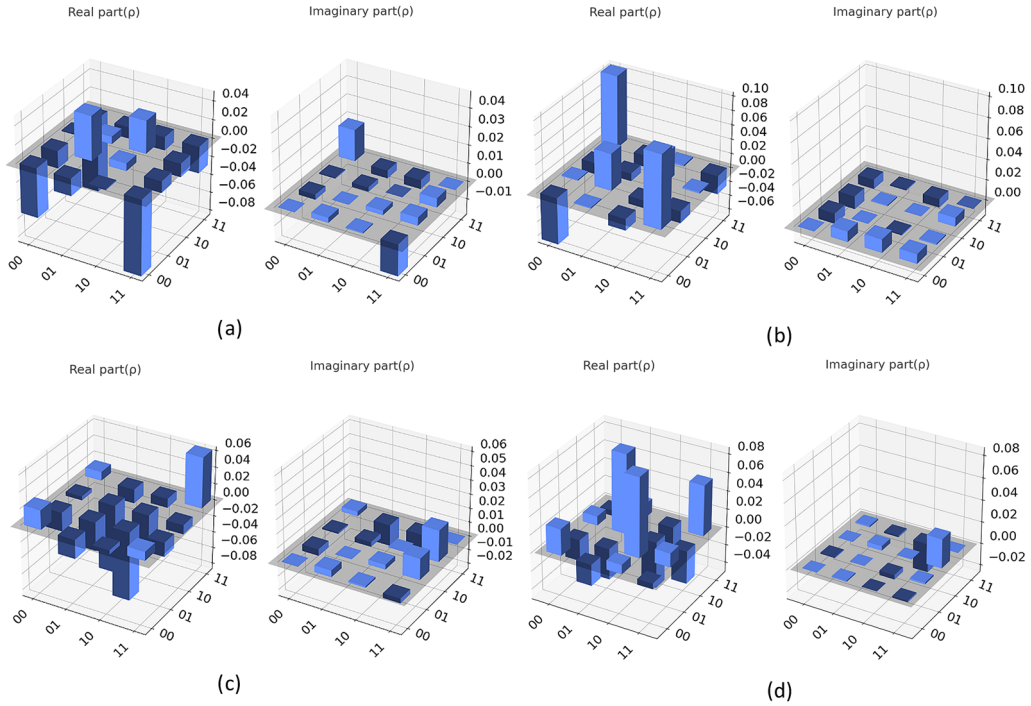

Figure 2. Differences between the density matrix measured by real quantum hardware ibm_brisbane and the density matrix from the Aer quantum simulator for the Bell set: (**a**) $|\Phi^+\rangle$; (**b**) $|\Phi^-\rangle$; (**c**) $|\Psi^+\rangle$; (**d**) $|\Psi^-\rangle$.

4. Results of Generalized n-Qubit GHZ States Preparation and Measurement

Experiments to measure the generalized GHZ states from Equation (7) on the default (Z) basis with a varied number of qubits involved in the state n = [3,5,8–10] were conducted on ibm_brisbane quantum machine. The number of shots in every experiment was 2000. Based on the counts N_0 revealing all zeros in the measurement $\left(|0\rangle^{\otimes n}\right)$ and counts N_1 yielding all ones from measurement $\left(|1\rangle^{\otimes n}\right)$, the probability $p\left(|0\rangle^{\otimes n}\right) + \left(p|1\rangle^{\otimes n}\right)$ was estimated as

$$p_{GHZ}(n) = p\left(|0\rangle^{\otimes n}\right) + p\left(|1\rangle^{\otimes n}\right) = \frac{N_0 + N_1}{N_{sh}} \tag{10}$$

with N_{sh} referring to the total shot count of 2000. The results are reported in Table 2 and plotted in Figure 3.

Table 2. Measured $p_{GHZ}(n)$ for different numbers of qubits. The n = 10 experiments were performed twice.

Qubits n	$p_{GHZ}(n)$
3	0.9600
5	0.8230
8	0.5395
9	0.0665
10	0.2490
10	0.1195

https://doi.org/10.3390/engproc2026122005

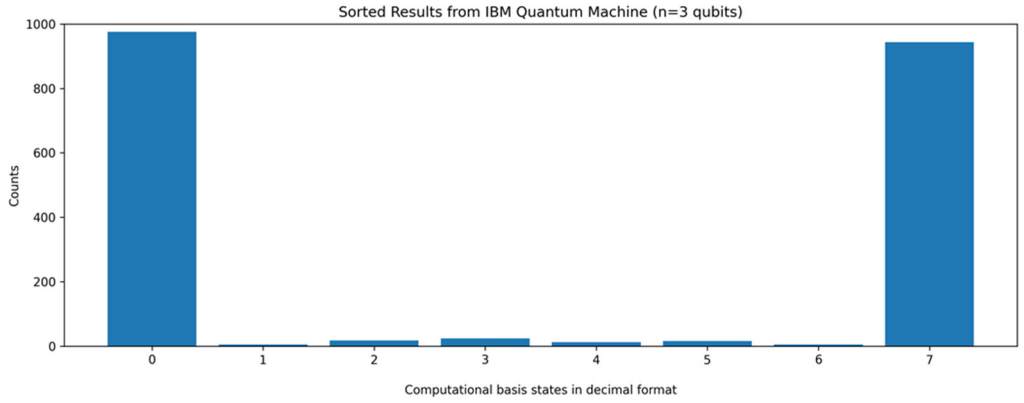

(**a**)

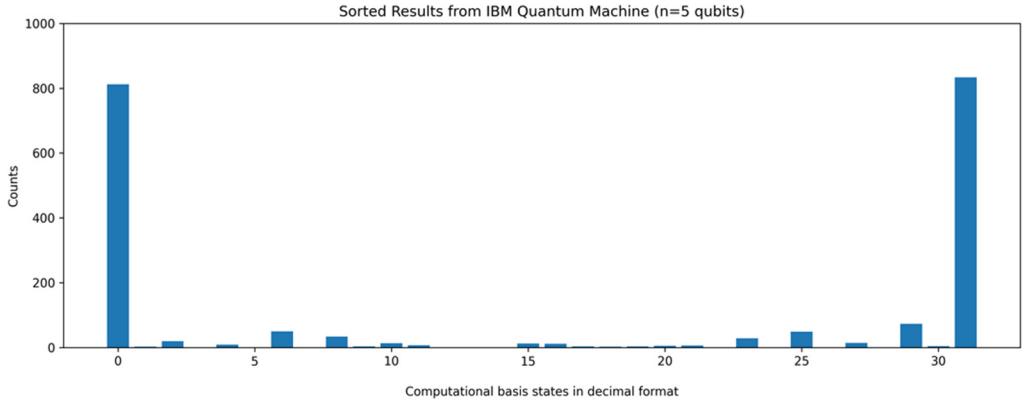

(**b**)

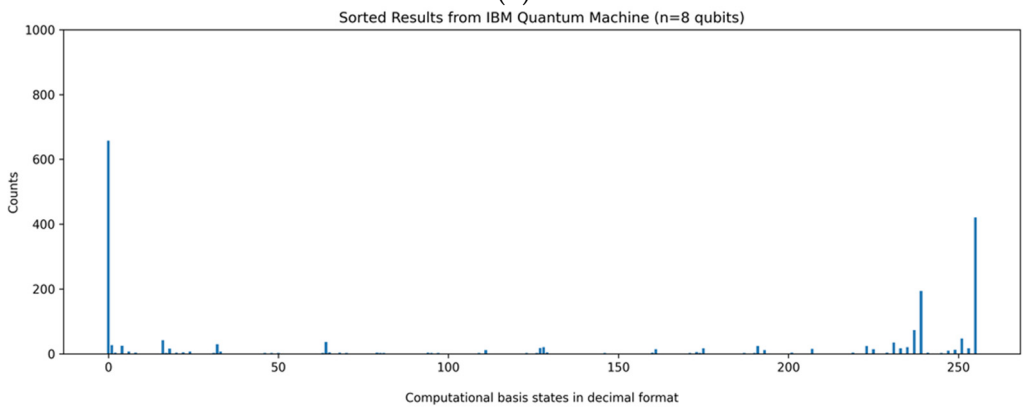

(**c**)

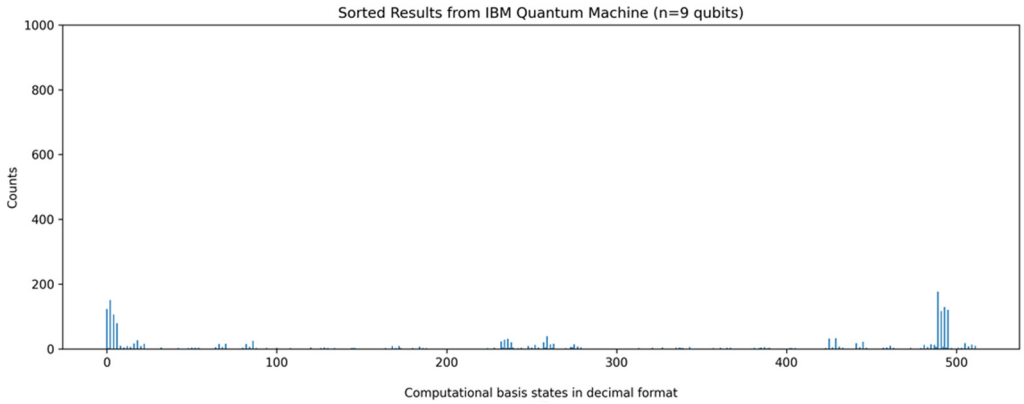

(**d**)

Figure 3. Measurement counts for GHZ states executed on ibm_brisbane: (**a**) results from IBM Quantum Machine at n = 3 qubits; (**b**) results from IBM Quantum Machine at n = 5 qubits; (**c**) results from IBM Quantum Machine at n = 8 qubits; (**d**) results from IBM Quantum Machine at n = 9 qubits.

Ideally, for the generalized GHZ state in Equation (7), $p_{GHZ} = 100\%$. In practice, even at $n = 3$ false counts were observed, corresponding to states other than the two expected outcomes $\left(|0\rangle^{\otimes n}\right)$ and $\left(|1\rangle^{\otimes n}\right)$. Nevertheless, the observed probability remained close to the ideal, with $p_{GHZ}(3) = 96\%$. At $n = 5$, the total counts for the two exclusive states dropped to 1646, giving $p_{GHZ}(5) = 82.3\%$. The probability continued to decrease approximately linearly with n, with the notable exception of $n = 9$, where $p_{GHZ}(9) = 6.65\%$ marked a sharp drop that deviated from the general trend. Probability $p_{GHZ}(n)$ versus the number of qubits is plotted in Figure 4. For n = 10, the plotted value corresponds to the mean of two experimental runs.

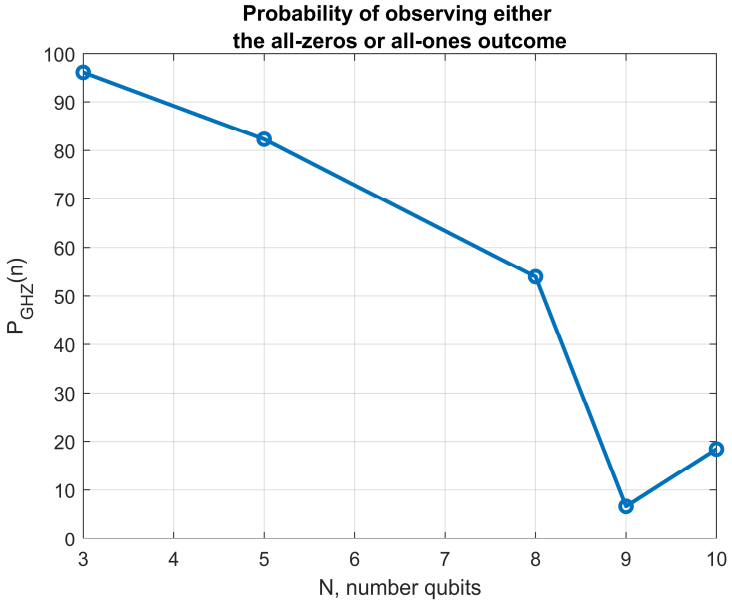

Figure 4. Probability $p_{GHZ}(n)$ vs. number of qubits.

The Qiskit program to generate and measure n-qubit GHZ states on IBM Quantum hardware was initialized with n qubits and an equal number of classical bits. A Hadamard gate was applied to the first qubit, followed by a chain of CNOT gates from the first to all the remaining qubits, creating the entangled GHZ state. All qubits were then measured within the computational basis and stored in the conventional bits. The circuit was transpiled for the selected IBM backend (here ibm_brisbane) and executed using 2000 shots. The output provides the empirical probabilities of the two GHZ basis states $|0\rangle^{\otimes n}$ and $|1\rangle^{\otimes n}$, together with the additional noise-induced outcomes.

States $|\Phi^+\rangle$, $|\Phi^-\rangle$, and $|\Psi^+\rangle$ as well as the generalized GHZ states were executed using an earlier Qiskit version [11], while the fourth Bell state $|\Psi^-\rangle$ was executed using an updated Qiskit release [12]. Ideally, only the two states to the extreme left $\left(|0\rangle^{\otimes n}\right)$ and to the extreme right $\left(|1\rangle^{\otimes n}\right)$ should be present.

The Jupyter notebooks implementing the quantum algorithms are provided in the Supplementary Materials.

5. Conclusions

This work demonstrated the preparation and quantum state tomography of the four standard Bell configurations on IBM's ibm_brisbane quantum computer as well as an assessment of performance with generalized GHZ states with up to 10 qubits.

The element-wise comparison between the experimentally reconstructed and the simulated density matrices for the four Bell states represents the discrepancies arising from

noise and device imperfections. These differences provide a more realistic assessment of hardware performance than quantum state fidelity values alone.

As the density matrix scales up, the entry count grows as 4^n, and its size quickly becomes unmanageable with the volume of qubits. The simplified procedure of observing the correct counts when the state detection is made in the default computational frame provides a straightforward way to assess the device's performance. The generalized GHZ-states experiment demonstrated that although the quantum processor ibm_brisbane has 127 qubits, a reliable entangled state involving a significant number of qubits (beyond 8) could not be achieved at the time of the experiment (October 2024), under the criterion that the "leakage" into incorrect measurement outcomes should not exceed 50%.

Supplementary Materials: The Jupyter notebooks implementing the quantum algorithms using Qiskit are openly available at https://github.com/quantum-tomography/quantum-tomography-GHZ (accessed on 13 January 2026) under the MIT License.

Author Contributions: Conceptualization, D.P.; methodology, D.P.; software, D.P.; validation, D.P.; formal analysis, D.P.; investigation, D.P.; resources, Y.S.; data curation, D.P.; writing—original draft preparation, Y.S.; writing—review and editing, Y.S.; visualization, Y.S.; supervision, Y.S.; project administration, Y.S.; funding acquisition, Y.S. All authors have read and agreed to the published version of the manuscript.

Funding: This study is co-financed by the European Union through the Program "Research, innovation and digitalization for smart transformation 2021–2027", project Center of Competence "Blue Coastal Marine and Riverine Innovative & Sustainable Management of Environments and Resources (Blue Cristal)", contract #BG16RFPR002-1.014-0016-C01.

Institutional Review Board Statement: Not applicable.

Informed Consent Statement: Not applicable.

Data Availability Statement: The experimental data presented in this study are openly available in the GitHub repository "quantum-tomography-GHZ" at https://github.com/quantum-tomography/quantum-tomography-GHZ (accessed on 13 January 2026). The repository includes all Jupyter notebooks implementing the quantum experiments, including Bell and GHZ-state preparation and tomography. Raw measurement data produced on the IBM ibm_brisbane quantum device are available within the corresponding notebook cells.

Acknowledgments: We acknowledge the use of IBM Quantum services for this work. The views expressed are those of the authors, and do not reflect the official policy or position of IBM or the IBM Quantum team.

Conflicts of Interest: The authors declare no conflicts of interest. The funders had no role in the design of the study; in the collection, analyses, or interpretation of data; in the writing of the manuscript; or in the decision to publish the results.

References

1. Arute, F.; Arya, K.; Babbush, R.; Bacon, D.; Bardin, J.C.; Barends, R.; Biswas, R.; Boixo, S.; Brandão, F.G.S.L.; Buell, D.A.; et al. Quantum supremacy using a programmable superconducting processor. *Nature* **2019**, *574*, 505–510. [CrossRef] [PubMed]
2. Upadhyay, S.; Alam, M.; Ghosh, S. Architectures for quantum information processing. *arXiv* **2022**, arXiv:2211.06449. Available online: https://arxiv.org/abs/2211.06449 (accessed on 21 January 2025).
3. Macchiavello, C. On the role of entanglement in quantum information. *Phys. A* **2004**, *338*, 68–75. [CrossRef]
4. Hauser, N.; Bayerbach, M.J.; D'Aurelio, S.E.; Weber, R.; Santandrea, M.; Kumar, S.P.; Dhand, I.; Barz, S. Boosted Bell-state measurements for photonic quantum computation. *NPJ Quantum Inf.* **2025**, *11*, 41. [CrossRef]
5. Ekert, A.K. Quantum cryptography based on Bell's theorem. *Phys. Rev. Lett.* **1991**, *67*, 661–663. [CrossRef] [PubMed]
6. Altepeter, J.B.; James, D.F.; Kwiat, P.G. 4 Qubit Quantum State Tomography. In *Quantum State Estimation*; Paris, M.G.A., Řeháček, J., Eds.; Springer: Berlin/Heidelberg, Germany, 2004; pp. 113–145.

7. Patel, A.D. The quantum density matrix and its many uses: From quantum structure to quantum chaos and noisy simulators. *J. Indian Inst. Sci.* **2023**, *103*, 401–417. [CrossRef]
8. Sisodia, M. Comparison the performance of five-qubit IBM quantum computers in terms of Bell states preparation. *Quantum Inf. Process.* **2020**, *19*, 215. [CrossRef]
9. IBM Quantum. Available online: https://quantum.cloud.ibm.com/ (accessed on 21 January 2025).
10. Javadi-Abhari, A.; Treinish, M.; Krsulich, K.; Wood, C.J.; Lishman, J.; Gacon, J.; Martiel, S.; Nation, P.D.; Bishop, L.S.; Cross, A.W.; et al. Quantum computing with Qiskit. *arXiv* **2024**, arXiv:2405.08810. [CrossRef]
11. IBM Quantum. Qiskit and IBM Runtime Tools (Versions: Qiskit 1.2.4, Qiskit Aer 0.15.1, Qiskit Experiments 0.7.0, Qiskit IBM Runtime 0.28.0) [Computer Software]. Available online: https://quantum.cloud.ibm.com/docs/en/api/qiskit/1.2 (accessed on 7 January 2025).
12. IBM Quantum. Qiskit and IBM Runtime Tools (Versions: Qiskit 1.3.1, Qiskit Aer 0.16.0, Qiskit Experiments 0.8.1, Qiskit IBM Runtime 0.34.0) [Computer Software]. Available online: https://quantum.cloud.ibm.com/docs/en/api/qiskit/1.3 (accessed on 21 January 2025).
13. Nielsen, M.A.; Chuang, I.L. *Quantum Computation and Quantum Information*; 10th Anniversary ed.; Cambridge University Press: Cambridge, UK, 2010. Available online: https://www.cambridge.org/core/product/01E10196D0A682A6AEFFEA52D53BE9AE (accessed on 21 January 2025).
14. Broadbent, A.; Chouha, P.R.; Tapp, A. The GHZ state in secret sharing and entanglement simulation. In Proceedings of the 2009 Third International Conference on Quantum, Nano and Micro Technologies (ICQNM), Cancun, Mexico, 1–7 February 2009; IEEE: Los Alamitos, CA, USA, 2009; pp. 59–62.
15. Adedoyin, A.; Ambrosiano, J.; Anisimov, P.; Casper, W.; Chennupati, G.; Coffrin, C.; Djidjev, H.; Gunter, D.; Karra, S.; Lemons, N.; et al. Quantum algorithm implementations for beginners. *ACM Trans. Quantum Comput.* **2022**, *3*, 1–92. [CrossRef]

Disclaimer/Publisher's Note: The statements, opinions and data contained in all publications are solely those of the individual author(s) and contributor(s) and not of MDPI and/or the editor(s). MDPI and/or the editor(s) disclaim responsibility for any injury to people or property resulting from any ideas, methods, instructions or products referred to in the content.